Lab on a Chip

PAPER

View Article Online
View Journal

Cite this: DOI: 10.1039/c4lc00057a

Automated single cell microbioreactor for monitoring intracellular dynamics and cell growth in free solution†

Eric M. Johnson-Chavarria,[a] Utsav Agrawal,[b] Melikhan Tanyeri,[b] Thomas E. Kuhlman[acd] and Charles M. Schroeder*[ab]

Received 15th January 2014,
Accepted 7th May 2014

DOI: 10.1039/c4lc00057a

www.rsc.org/loc

We report an automated microfluidic-based platform for single cell analysis that allows for cell culture in free solution with the ability to control the cell growth environment. Using this approach, cells are confined by the sole action of gentle fluid flow, thereby enabling non-perturbative analysis of cell growth away from solid boundaries. In addition, the single cell microbioreactor allows for precise and time-dependent control over cell culture media, with the combined ability to observe the dynamics of non-adherent cells over long time scales. As a proof-of-principle demonstration, we used the platform to observe dynamic cell growth, gene expression, and intracellular diffusion of repressor proteins while precisely tuning the cell growth environment. Overall, this microfluidic approach enables the direct observation of cellular dynamics with exquisite control over environmental conditions, which will be useful for quantifying the behaviour of single cells in well-defined media.

Introduction

The ability to quantify gene expression and intracellular dynamics at the single cell level has opened up new vistas in genomics and proteomics. Single cell analysis allows for characterization of heterogeneous variability within isogenic cell populations that cannot be observed using bulk methods. Traditional approaches for studying gene expression have relied on high-throughput screening assays such as flow cytometry, which allows for single cell resolution.[1] However, these methods typically require large volumes (~1–10 mL) of cell culture and growth media, which may not be advantageous to limited sample volumes or fragile cell lines. In addition, flow cytometry provides information at an instant in time, rather than a dynamic time course of data from a single sample over long time scales.

Recent advances in microfluidics and microscopy have enabled the real-time investigation of gene network dynamics. Microfluidic flow cells manually constructed from adhesive or parafilm sandwiched in between glass coverslips are commonly used in single molecule and single cell research. However, it is difficult to achieve small channel geometries (<500 μm) using this approach, and these methods are generally limited in the ability to precisely control nutrient conditions in a rapid, reliable, and time-dependent fashion.

Microfluidic fabrication has allowed researchers to design and build devices for single cell analysis, thereby enabling studies of gene expression,[2] chemotaxis, enzymatic activity using chemical cytometry,[3,4] and cell sorting in free solution.[5–9] Nutrient or chemical gradients can be readily generated in low Reynolds number laminar flows within microfluidic channels. Moreover, the elastomeric properties of polydimethylsiloxane (PDMS) have allowed for fabrication of on-chip valves, which allows for flow metering and delivery of cells into microfluidic chambers or careful control over nutrient streams.[10,11] To this end, feedback control has been coupled with on-chip valves to generate an automated microfluidic Wheatstone bridge for on-demand capture of samples for rapid analysis.[12] Microfluidic platforms have also been used to study chemotaxis *via* time-dependent control over chemical gradients.[13] In addition, microcavities have been used to build single cell microarrays that allow for the adherence of one cell per cavity[14,15] or many cells per chamber, including a mother cell and subsequent lineage.[16] However, the aim of the present work is to remove

[a] *Center for Biophysics and Computational Biology, University of Illinois at Urbana-Champaign, Urbana, IL, USA*
[b] *Department of Chemical and Biomolecular Engineering, University of Illinois at Urbana-Champaign, 600 S. Mathews Ave., Urbana, IL, USA.*
E-mail: cms@illinois.edu; Fax: +1 (217) 333 5052; Tel: +1 (217) 333 3906
[c] *Department of Physics, University of Illinois at Urbana-Champaign, Urbana, IL, USA*
[d] *Center for the Physics of Living Cells, University of Illinois at Urbana-Champaign, Urbana, IL, USA*

† Electronic supplementary information (ESI) available: Details on microdevice fabrication, mask design file, and implementation of the SCM are provided. Details on the bacterial strains used in this work are provided. Videos of single cell experiments are also provided. See DOI: 10.1039/c4lc00057a

physical barriers and confine cells in free solution for extended time scales.

The ability to integrate single cell experimental data and large-scale simulations for predicting whole cell phenotypes is a central goal in the field. Combined experimental and simulation-based approaches are required to understand the complex dynamics of cellular systems. Within a genetically-identical population of cells, intrinsic noise from gene expression can induce phenotypic heterogeneity. Recently, stochastic 'noise' within the *lac* circuit has been incorporated in a whole cell simulation.[17,18] In addition, chemotactic receptor adaptation times have been modeled to investigate optimal filtering as dictated by the cut-off frequency of a low-pass filter,[19] which responds to low frequency but not to high frequency nutrient fluctuations. Interestingly, this type of response is essential for a cellular system to adapt or to sustain fitness in rapidly fluctuating environment conditions.

Overall, there is a critical need for development of improved techniques for single cell analysis. These methods can provide fundamentally new information on cell dynamic variation and can be coupled with large-scale models for holistic approaches to understanding genetic network dynamics. Current microfluidic-based approaches for single cell analysis can be classified into two categories: contact and non-contact based methods. Contact based methods for trapping include barrier hydrodynamics and chemical–gel matrices.[20–22] Non-contact based methods isolate target cells by using optical, electric, acoustic, or magnetic fields.[23,24]

Optical tweezers are a common method for non-contact particle trapping and are commonly used for single molecule and single cell experiments.[25] Optical trapping allows for passive trapping of particles, wherein focused light enables confinement without the need for continuous feedback control.[26] Recently, this method was used to study the chemotactic motion of single *Escherichia coli* cells using a dual trap to confine the poles of a single cell.[27] Min *et al.* furthered the use of this technique to observe run and tumble statistics of single *E. coli* cells.[28] Although optical tweezers provide a convenient method for trapping, the use of a focused laser beam to confine living cells for long time scales has raised concerns about local heating and irradiative photo-damage to cellular structures.[29] In prior work, potential damage due to energy exposure was mitigated using an enzymatic oxygen scavenging system to generate anaerobic conditions, which minimized the formation of free radical singlet oxygen species.[30]

Irradiative damage was also previously investigated by Ayano *et al.* using optical tweezers to transport single cells to micro-chamber arrays.[31] These authors observed that continuous exposure of cells to 3 mW of laser illumination for 3 h resulted in complete stoppage of cell growth. Indeed, light exposure to living cells during these experiments is considerable. As a reference, consider the use of time-lapse fluorescence microscopy to illuminate cells with a mercury arc lamp (~15 mW). Here, an exposure time of 0.25 s (*e.g.*, acquiring 15 frames at 60 fps) results in a total energy accumulation of 3.75 mJ across the field of view. The reported lower limit of energy required for optical trapping focused at a specific target is ~6 mJ.[32]

Using contact based trapping methods, researchers have relied on advances in microfluidic fabrication to trap cells using hydrodynamic barriers. In these devices, cells are commonly captured in arrays while continuously exchanging media through the array,[33] which allows for multiplexed screening of cells with nutrient exchange. In many cases, barriers are well suited to study cell-to-cell dynamics with large cell loading per well, rather than a single cell per trapping site. Researchers have also used non-contact hydrodynamic methods based on micro-eddies to trap cells, wherein rotational flow is used to confine cells within micro-vortices or against a pillar barrier. The forces exerted by these techniques have been reported to be ~30 pN with shear stresses $\leq$1.5 N m^{-2} (15 dyn cm^{-2}), which is comparable to arterial blood flow.[24,34,35] Alternative non-contact methods have relied on magnetic force fields,[36] acoustic traps,[37] or electric fields to trap particles.[38,39] However, magnetic trapping of cells generally requires intracellular embedding of ferromagnetic particles, which can be perturbative. Moreover, electric field trapping requires special considerations regarding the electrical conductivity of the media and may perturb cell membrane electrical potentials.

Overall, there is a strong need for development of new non-contact based methods for single cell analysis. In particular, new microfluidic platforms are required that allow for chemostatic growth environments for single cells, with the ability to control cellular growth media and to observe cell dynamics. In this paper, we report the development of a single cell microbioreactor (SCM) that allows for the investigation of cell growth in free solution with the combined ability for time-dependent control over media conditions (Fig. 1). We use the SCM to characterize cell growth dynamics in free solution, and in all cases, single cell experiments are compared to bulk growth (see ESI†). In addition, we also use the SCM to investigate dynamic gene expression and intracellular spatial distributions of transcription factors in single bacterial cells under precise dynamic control over environmental conditions.

Materials and methods

Microdevice fabrication

We use standard soft-lithography techniques based on PDMS[40] to fabricate two-layer microfluidic devices capable of generating a planar extensional flow, which facilitates cell trapping. The master molds for the fluidic and control layers are created by spin coating a negative photoresist (SU8, MicroChem) on silicon wafers to a thickness of 30 μm and 100 μm, respectively. For the fluidic layer, we added a diamond shaped feature (>60 μm thickness) at the centre of the cross-slot geometry, which provides a raised 'ceiling' for decreasing the background signal during imaging. Casting the fluidic and control layers in PDMS was prepared using a 15 : 1 and 5 : 1 ratio of base to cross-linker,

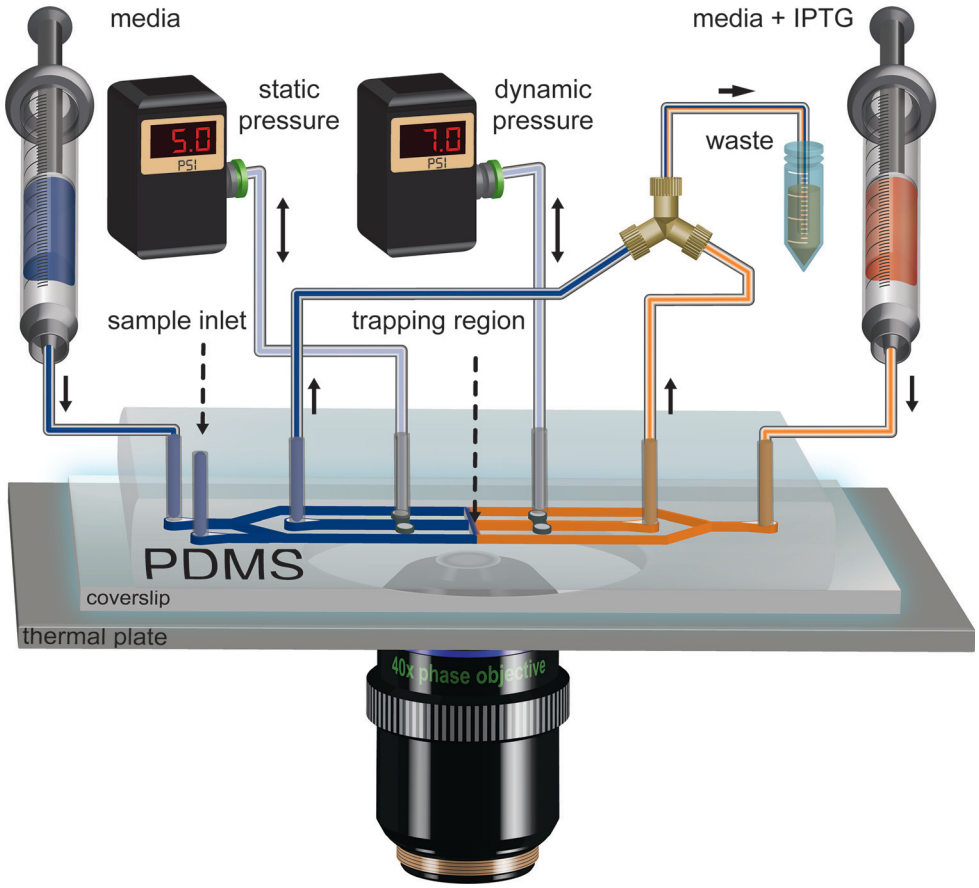

Fig. 1 Schematic of the single cell microbioreactor (SCM). The integrated device consists of several key components including: computer-controlled pressure regulators for controlling valve pressure, computer-controlled syringe pumps for delivering media into the device, and a thin-film thermal plate heater positioned underneath the device with thermocouple for controlling the temperature. The microfluidic platform is mounted on an inverted microscope equipped for phase-contrast and fluorescence imaging. The device allows for two distinct inlet media streams with a separate inlet for sample delivery. Device components are integrated and controlled using a custom LabVIEW program.

respectively. To fabricate the microdevice, PDMS is spin-coated onto the fluidic layer master (~100 μm thickness) and poured in a petri dish onto the control layer master (~5 mm thickness). Overall, the raised 'ceiling' provides a homogenous background, which facilitates image processing for detecting the cell centroid in phase-contrast microscopy (see ESI†).

The SCM consists of two inlet channels that converge at a cross-slot and diverge through two orthogonal outlet channels (Fig. 2). This cross-slot geometry generates a planar extensional flow with a stagnation point. Cells are trapped in free solution using automated feedback control over the position of the stagnation point, which can be precisely moved along the outlet direction by pressurizing/depressurizing on-chip membrane values located in the control layer. On-chip valves are positioned above the outlet channels in the fluidic layer and consist of a ~70 μm thick PDMS membrane. The thickness of the membrane valve can be varied during fabrication, which can be used to tune valve response.[41] Finally, a sample inlet stream is used to introduce cells into the SCM and is operated using an off-chip T-valve.

Experimental setup

A schematic of the single cell microbioreactor is shown in Fig. 1. The integrated device is mounted on an inverted microscope (Olympus IX-71) equipped for dual fluorescence and phase-contrast imaging. Custom LabVIEW software is used to integrate the main components of the system, including: (1) two CCD cameras for image acquisition, (2) software for image analysis and particle tracking, (3) a feedback controller for centroid trapping and single cell manipulation, and (4) two syringe pumps for dynamic control over the flow rates in the inlet media streams. During trapping, cells are imaged using phase-contrast microscopy facilitated by a 40× phase objective lens and a CCD camera (Applied Vision Technologies). Cell position is determined using an edge detection threshold and a custom-built particle analysis algorithm in LabVIEW. In this way, the user defines a region of interest (ROI) within the imaging window to establish a set point and spatial limits for real-time image processing within the field of view. A linear search algorithm is used to target and trap the cell that is closest to the centre of the ROI.

Hydrodynamic trapping is used to confine single cells, as previously described.[42,43] In brief, cells are maintained at a

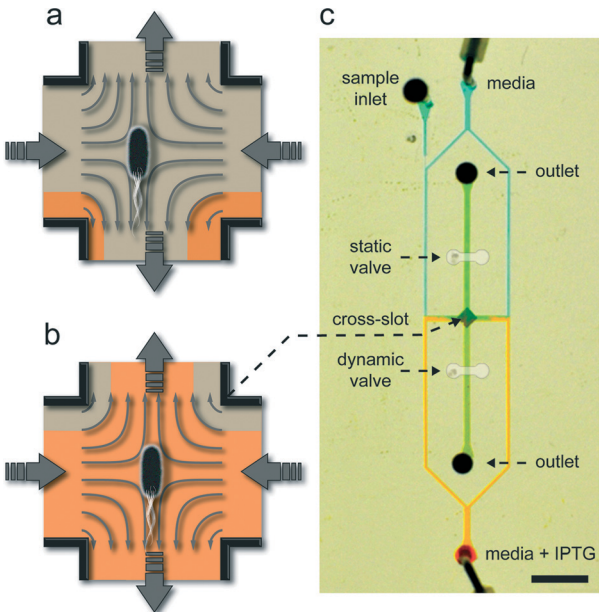

Fig. 2 Microfluidic device and schematic of trapping mechanism in the SCM. (a, b) Schematics of cell confinement in cross-slot region (not to scale), and the transitioning of growth environments from medium A to medium B. (a) A single cell is initially grown in medium A (tan color), followed by (b) rapid switching of the cell environment to medium B (orange color) while confining the cell in free solution (see Movie S1†). (c) Optical micrograph of the SCM. Scale bar: 3 mm.

set point position in free solution by continuously repositioning the location of the fluid stagnation point by pressurizing/de-pressurizing one of the on-chip membrane valves, known as the control valve. For this experiment, the control valve is set to an initial pressure (~7 psi) above the fixed offset pressure (~5 psi) of the static valve. Pressurizing the control valve tends to constrict the underlying fluidic channel, which moves the stagnation point in the direction of the outlet channel containing the control valve. A feedback controller determines instantaneous pressure values for trapping, which are actuated using off-chip pressure transducers (Proportion Air) connected to a BNC block. Dynamic control over media and nutrients is achieved using two syringe pumps (Cole Parmer and Harvard Apparatus PHD 2000), with both controlled using an integrated LabVIEW code. In this way, the user can specify "waveforms" of media generated by two distinct inlet streams, for example, a square wave signal of inlet A and inlet B with a 50% duty cycle. In all cases, the total volumetric flow rate in the microdevice is maintained at a constant value while cycling between fluid flow driven by the two syringe pumps (inlet A or inlet B), as shown in Fig. 1.

To facilitate time-lapse fluorescence microscopy (TLFM), an EMCCD camera (Andor-Solis) is used to capture fluorescence images of single cells at user-defined durations (5 min). Computer-controlled mechanical shutters (Uniblitz) are used to switch between phase-contrast and fluorescence imaging rapidly without compromising trap stability. Both CCD cameras are mounted on the trinocular port of the microscope.

The SCM is a nearly fully automated system. During data acquisition, manual user adjustments are limited only to coarse focusing (*z*-direction) and fluorescence intensity illumination. Finally, the SCM is temperature-controlled using thin film heaters (Thermofoil, Temflex Controls) positioned underneath the coverslip. The microdevice was calibrated to ensure that the fluidic streams are maintained at the desired set-point temperature (see ESI†). On-chip temperature is monitored using a thermocouple mounted below the cross-slot region of the SCM, and adjustments can be made to control temperature in a range between 25–42 °C.

Flow field kinematics in the cross-slot region

To achieve particle confinement using hydrodynamic trapping, we incorporated a cross-slot geometry into the design of the microfluidic device, as previously developed in our lab.[41–43] The cross-slot geometry generates a planar extensional flow, which is both irrotational and solenoidal as specified by the curl and divergence of the velocity vector field $\vec{V}$ at any point ($\nabla \times \vec{V} = 0, \nabla \cdot \vec{V} = 0$). This flow field is specified by a velocity potential φ and stream function ψ:[44]

$$\varphi = \frac{\dot{\varepsilon}}{2}\left(y^2 - x^2\right);\ \psi = \dot{\varepsilon} yx \tag{1}$$

where

$$\frac{\partial \varphi}{\partial y} = \frac{\partial \psi}{\partial x},\ \frac{\partial \varphi}{\partial x} = -\frac{\partial \psi}{\partial y} \tag{2}$$

and the partial derivatives of the velocity potential or stream function yield the velocity vector components:

$$v_x = \frac{\partial \varphi}{\partial x} = -\frac{\partial \psi}{\partial y},\ v_y = \frac{\partial \varphi}{\partial y} = \frac{\partial \psi}{\partial x} \tag{3}$$

The velocity vector is described as $\vec{V} = \dot{\varepsilon}(-x, y)$, where $\dot{\varepsilon}$ is the strain rate and x and y are the Cartesian coordinates along the inlet and outlet directions, respectively, relative to the stagnation point position. In brief, pressurization/de-pressurization of the on-chip control valve varies the flow resistance in one of the outlet channels relative to the opposing outlet stream, which allows for fine-scale control over the stagnation point position. In this way, single cells can be trapped in free solution by active flow control. Finally, it should be noted that cell trapping in 2D is achieved by controlling a single parameter (relative flow rates in an outlet channel along the extensional flow axis). The inlet flow direction (compressional axis) is a stable trapping direction, which does not require active feedback control. In this way, the flow field can be described as a saddle surface by the velocity potential function φ, wherein the outlet direction (extensional axis) is the unstable flow direction requiring active feedback control for trapping.

Automated feedback controller

For proof-of-principle trapping of non-motile particles (~2.2 μm diameter polystyrene beads, see Movie S1†), we used a simple proportional feedback controller:[45]

$$p_i(t) = p_{i-1} + K_c e_i(t) \quad (4)$$

where p_{i-1} is the offset pressure, K_c is the dimensionless proportional gain value, and $e(t)$ is the error defined as:

$$e(t) = y_{sp} - y_m(t) \quad (5)$$

where y_{sp} and y_m are the set point and instantaneous cell centroid positions, respectively. We found that the proportional controller resulted in robust and stable trapping for micron-sized and sub-micron particles, as previously demonstrated.[42,43,46,47] For trapping motile bacterial cells, we implemented an adaptive controller with a gain schedule defined by a custom rule base (see ESI†). In brief, the adaptive controller is based on a proportional controller, while additionally accounting for changes in particle position, direction, and speed relative to the previous iteration in the feedback loop. For example, if a particle is increasing in speed and moving away from the set point position, then the controller uses a larger value of the gain K_c to reposition the particle to the set point. However, if a particle is moving towards the set point, then a smaller value of the gain is used. We observed that this controller results in stable trapping of single motile cells for long time scales, and is generally robust to perturbations in fluid flow. Trap stability is essential for implementing dynamic "on-demand" nutrient exchange using the synchronized syringe pumps controlled by LabVIEW.

E. coli cell culture and preparation for gene expression

For growth analysis experiments, we used *E. coli* strains MG1655 and BLR(DE3). Overnight cell cultures were grown in LB (Lysogeny Broth) medium + 100 μg mL^{-1} ampicillin inoculated from a single colony on an LB agar plate. Following overnight culture in an incubated shaker at 37 °C, the starter culture was diluted 1 : 100 in fresh LB medium + ampicillin. The serially diluted sample was then cultured for 3 h on an incubated shaker at 37 °C. Next, the cell samples are introduced into the microfluidic device to monitor cell growth during trapping in free solution at a constant flow rate.

For real-time gene expression experiments, standard PCR and ligation techniques were used to clone a gene encoding for a variant of the yellow fluorescent protein (Venus) downstream of two *lac* operators on a strong T5 promoter (Qiagen, pQE80L plasmid). Cloning was performed using BLR(DE3) competent cells (a derivative of BL21), which improves exogenous plasmid yields. Cells were transformed with plasmid vectors using heat shock method. For preparing cells for on-chip experiments, the BLR strain was cultured using identical methods used for growth experiments, except that cells from overnight cultures were diluted 1 : 100 in M9 minimal media with 0.5% v/v glycerol + ampicillin. The media used for inducing gene expression contained 1 mM IPTG (an allolactose mimic) and was otherwise identical to initial media conditions (M9 minimal media with 0.5% v/v glycerol + ampicillin).

Results and discussion

Observing cell growth dynamics for long time scales

We used the SCM to observe the growth of single living *E. coli* cells in free solution for extended periods of time (up to ~5 doubling times) (Fig. 3). Overnight cultures were diluted into fresh LB medium, grown, and delivered into the SCM through the sample inlet stream (Fig. 2). Pure LB medium (LB + ampicillin) was delivered through the two media inlet streams (Fig. 2), while maintaining the device at 37 °C. During cell trapping and growth experiments, the sample inlet stream was closed, and a constant volumetric flow rate of 100 μL h^{-1} was maintained in the two inlet media streams to facilitate flow-based trapping of single cells in solution. Based on the flow field kinematics and the applied flow rates, we estimated the average shear stress experienced by a single cell due to flow (see ESI†). Due to laminar flow conditions in the microdevice and the confinement of cells at a zero-velocity position (stagnation point), the average shear stress is ~1×10^{-2} dyn cm^{-2}, which is two orders of magnitude smaller than the shear stress cells experience when grown in a large volume shaker flask.[48]

For cell growth experiments, the controller gain constant K_c was set to ensure robust cell trapping, but was generally not fine-tuned to maximize trap stiffness. We found that these 'relaxed' trapping conditions were more robust to flow perturbations, which are generally uncommon, but are important to consider during long time scale trapping experiments (~4+ hours). In any case, the feedback controller can be fine-tuned to yield a tighter trap stiffness, if desired. In addition, a cell trapped in the 2D image plane is free to diffuse in the *z*-direction, defined as the direction perpendicular to the image plane. At the beginning of a cell growth experiment, single cells are selected at the mid-plane of the fluidic channel. During the course of an experiment, cells traverse ±20 μm from the centre plane of the channel (see Movie S2, S3†). The flow profile in the *z*-direction is parabolic in shape, which leads to a factor of ~2× change in the local flow rate of the cell, which has relatively minor effect on the applied shear force due to flow. Finally, to facilitate phase-contrast imaging during single cell trapping experiments, we modified the fluidic channel geometry to incorporate an increased channel height at the cross-slot, which reduced background intensity due to PDMS boundaries (see ESI†).

Growth analysis was performed by tracking cell length as a function of time (Fig. 3a and b). Cells were observed to increase in size over time, followed by a distinct cell division event. Following cell division, we generally chose to trap and retain one of the daughter cells, and the second cell is advected away into the waste stream. In LB medium, *E. coli* showed a mean doubling time of ~42 min in the SCM

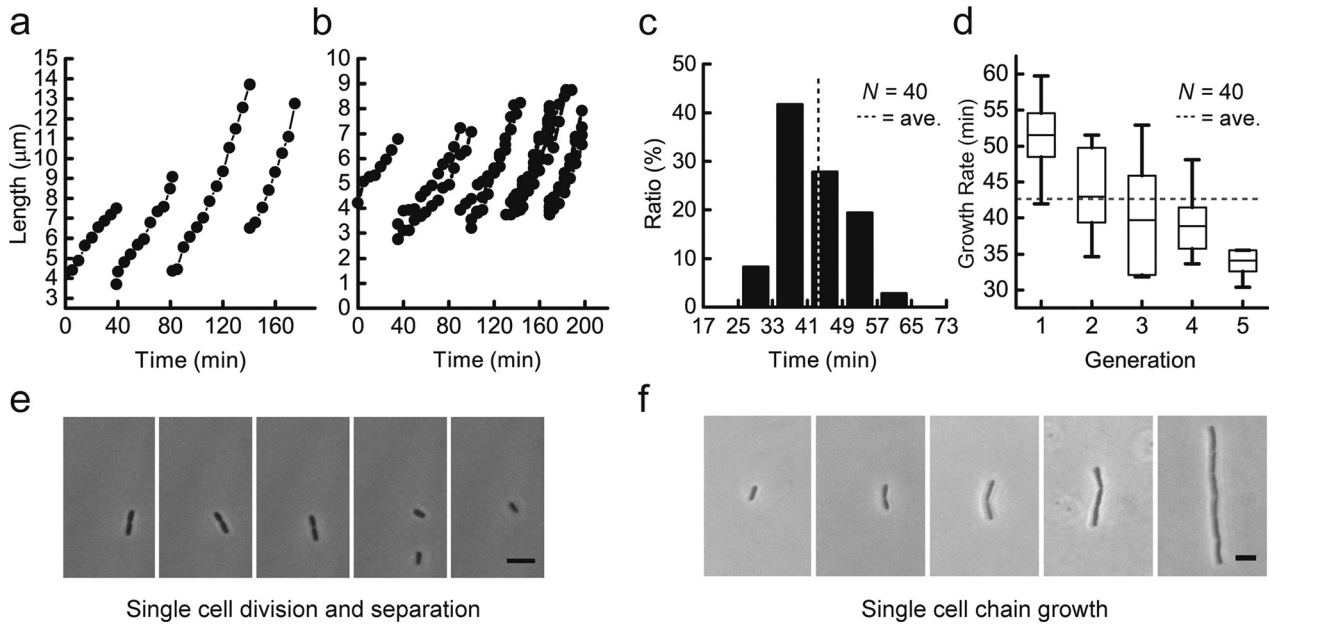

Fig. 3 Single cell growth dynamics monitored over long time scales using the SCM. (a, e) Single cell growth trajectory and time-lapse images for a cell growth event. For dividing cells, the user has the ability to select, trap, and continue experiments with one of the daughter cells. (b, f) Multiple cell growth trajectories and time-lapse images originating from a single cell growing in a filamentous morphology (see Movie S2, S3†). (c) Histogram of doubling times showing an average of 42.5 min (dotted line, N = 40 cells). (d) Box plot of doubling times over multiple cell generations in the SCM. Whiskers denote the min and max of growth rates and box boundaries are the 25th and 75th percentile with line indicating the mean of each generation. (e, f) Time-lapse phase-contrast images of cell growth trajectories quantified in (a) and (b), respectively. Scale bars: 5 μm.

(average of 40 cells) (Fig. 3c). Interestingly, by observing the lineage of a single cell over multiple doubling times, the SCM allows for quantification of growth rates as a function of generation number (Fig. 3d).

In general, single cell experimental data is consistent with bulk analysis performed using absorbance measurements in a 96 well plate format (see ESI†). In bulk experiments, the doubling time of *E. coli* was found to be ~60 min in LB medium and ~111 min in M9 minimal media at 37 °C (see ESI†). Determining growth rates in single cell measurements (*via* cell length) is fundamentally different than determining growth rates in bulk experiment (*via* absorbance at 600 nm), which leads to slight differences in these quantities. The SCM provides a chemostatic environment by continuous delivery of fresh nutrients with continuous removal of metabolic excretion of by-products. In this way, single cells in the SCM are not affected by population-level signaling or cell crowding through a mechanism of quorum-sensing that occurs in dense cell cultures in bulk experiments.[9,49,50] Moreover, bulk measurements of cell growth may be prone to evaporation in 96 well plates, wherein individual wells are open to the atmosphere. Evaporation can be mitigated by floating a layer of oil on top of each well, but this approach can induce anaerobic growth conditions. In our observation, this effect has only been observed at time scales beyond the log phase.

In addition to cell growth measurements, the SCM also allows for direct observation of cell shape and phenotype during growth. Interestingly, we observed different phenotypes for *E. coli* cells that were initially prepared from stationary state cultures compared to those that were prepared from log-phase cultures. Cells prepared from log phase cultures that are preconditioned by avoiding changes in media before entering the SCM divide readily, with mother cells dissociating from their progeny (Fig. 3e). On the other hand, cells from stationary state cultures were prone to grow in long filamentous chains with distinct cellular poles with each division (Fig. 3f). This behaviour can be attributed to a combination of the fluid flow in the microchannel and initial growth state of the target cell. For both cases (filamentous *versus* non-filamentous growth), however, the average growth rates were similar as a function of generation number. Throughout our experiments, cells were cultured and induced under aerobic conditions. PDMS is highly permeable to oxygen,[51] and the SCM intrinsically provides continuous replenishment of nutrients and dissolved oxygen during cell growth. In a series of experiments, we used an oxygen sensitive dye (resazurin) to determine that the concentration of dissolved oxygen in the fluidic streams facilitated cell growth under aerobic conditions (not shown). Overall, cells appeared to adapt to the chemostatic growth environment in the SCM over subsequent generations, which is shown in the average increase in growth rate with increasing generation number (Fig. 3d). The increase in growth rate suggests that cells are adapting to the chemostatic environment of the SCM, which is useful for long-term observation of single cell growth dynamics in free solution.

Gene expression: step-change in inducer concentration

In addition to cell growth experiments, we studied gene expression in single *E. coli* cells using TLFM and a

fluorescent reporter protein (Venus) as a proxy for gene expression (Fig. 4). For these experiments, we directly observed intracellular levels of fluorescence in single cells upon switching the growth medium surrounding a single cell from M9 minimal media with 0.5% v/v glycerol to M9 with glycerol + 1 mM IPTG (Fig. 4a, top panel). M9 media was chosen as the preferred growth medium for these experiments due to low levels of auto-fluorescence. A major advantage of the SCM is a precise and accurate knowledge of the initial time in the experiment (time zero in Fig. 4a, top panel), defined as the time at which the growth environment surrounding a cell is exchanged from one well-defined medium to a second well-defined medium. The transition time for exchanging the medium around a single cell is on the order of the inverse strain rate $\dot{\varepsilon}^{-1}$ (~1 s).

Upon transitioning cells to media containing IPTG, gene expression was induced by a standard double de-repression mechanism (Materials and methods). In brief, *E. coli* was transformed with a plasmid containing a strong T5 promoter regulated by two *lac* operators (see ESI†). In the absence of the IPTG inducer, this plasmid enables tight repression that minimizes the basal level or leaky expression of the fluorescent protein. At the beginning of each experiment, we targeted and trapped cells with low levels of intracellular fluorescence, such that the fluorescence intensity was approximately equal to the background signal. During these experiments, we first observed single living cells in M9 media without inducer for ~10 min, followed by switching the media surrounding a cell to M9 containing IPTG (see Movie S4†). In bulk experiments, cell growth was monitored using a 96 well plate assay. For these experiments, cells were induced with IPTG after culturing cells for ~300 min, which is roughly the time point at which cell growth can be detected and quantified using absorbance as a probe for cell density at a wavelength of 600 nm (see ESI†).

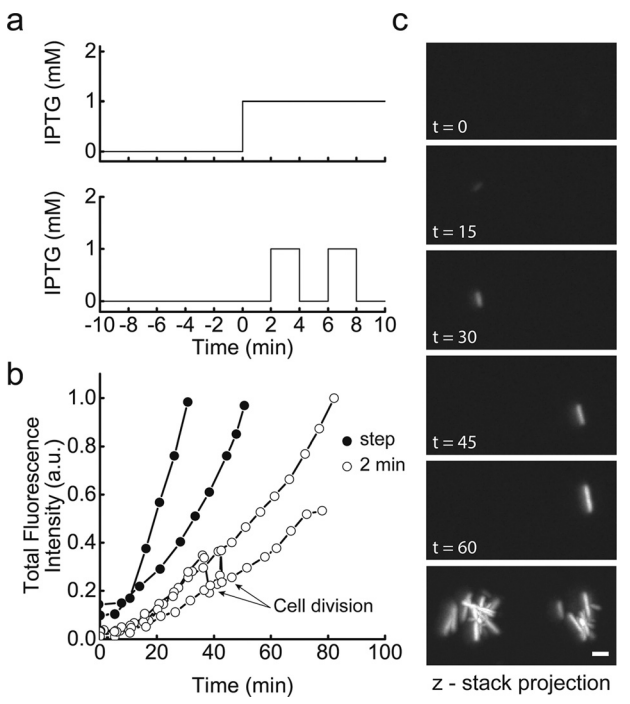

Fig. 4 Quantifying intracellular gene expression upon rapid environmental changes in the SCM. (a) Time-dependent concentration profiles of inducer (IPTG), showing a single step change (top panel) and a periodic step change with a 2 min period (bottom panel, see Movie S4†). (b) Intracellular fluorescence intensity following a single step change or periodic step change in IPTG. Cell division is denoted by a decrease in fluorescence due to a decrease in cell volume after division. Fluorescence is continuously monitored after cell division. (c) TLFM images of a single cell undergoing periodic step change in IPTG (2 min period) for 1 h. The bottom image contains a *z*-projection stack over the time course of the experiment. During a change in the cell environmental conditions by switching the inlet flow streams, a cell moves ~20 μm laterally along the compressional axis due to the asymmetric flow design in the device (see text for details). Scale bar: 5 μm.

Using this approach, we recorded the intracellular fluorescence intensity values after a single step change in cell growth media (from 0 to 1 mM IPTG) at 5 min intervals using TLFM. In all cases, we observed an exponential increase in intracellular fluorescence intensity, but the rate of increase was dependent on the cell growth rate over an ~80 min observation time period (Fig. 4b). Differences in the rate of increase in intracellular fluorescence levels can be attributed to slight differences in individual cell growth rates or small differences in initial cell dimensions. For these experiments, single cell growth rates varied within the general range of ~80–100 min in M9 media. We observed that single cell growth rates did not significantly vary between growth in M9 medium or M9 medium + 1 mM IPTG. Finally, we performed a series of control experiments to ensure that TLFM imaging conditions resulted in no significant amounts of photobleaching. To characterize the effect of photobleaching, we observed intracellular fluorescence levels in single cells pre-induced with M9 + 1 mM IPTG, followed by a switch to M9 medium without IPTG. During the first 10 min, the total fluorescence signal decreased due to cell division, followed by a slight decrease for longer time windows (>100 min). The slight decrease in fluorescence over long time scales can be attributed to cell growth and dilution of the fluorescent protein (see ESI†).

Gene expression: periodic 'forcing' of inducer concentrations

Following single-step change experiments, we studied the response of single cells to periodic, time-dependent 'forcing' functions or 'waveforms' in inducer concentration. In these experiments, we exposed cells to a periodic square wave signal of on/off induced states (1 mM/0 mM IPTG, respectively) with a 2 min period in the cycle. Periodic forcing experiments showed a difference in intracellular fluorescence levels over the course of 80 min compared to single-step change experiments (Fig. 4b). In particular, periodic forcing experiments appeared to show a delay in the onset of gene expression by ~5 min. In addition, we generally observed a slower rate of increase in fluorescence intensity for periodic step changes in inducer concentration compared to a single step change (Fig. 4b). Finally, we prepared an integrated time series of

fluorescence images obtained from single cells during the course of a periodic step change experiment, which amounts to a *z*-projection stack or time series of the fluorescence emission (Fig. 4c, bottom image). Due to the presence of the sample inlet channel on one side of the microdevice, there is a miniscule imbalance in the flow rates on either side of the device, which results in a slight shift in the *x*-position of a single cell (conveniently denoting a switch in growth medium), which can be seen in Fig. 4c. Overall, these experiments provide proof-of-principle demonstration of precise, time-dependent control over cell environmental conditions, coupled with simultaneous phase-contrast imaging and TLFM, for observing dynamic gene expression at the single cell level.

Intracellular protein diffusion experiments

To further demonstrate proof-of-principle operation of the SCM, we used the platform to observe intracellular diffusion of transcription factor proteins upon rapid exchange of cell growth media (Fig. 5). In particular, we directly observed the unbinding dynamics of Tet repressor proteins (TetR) fused with YFP (Venus) from a tandem binding array incorporated in the *E. coli* chromosome at the aptI locus (see ESI†).[52,53] Initially, cells are grown in media containing a glycerol carbon source (EZ Rich Defined Medium (RDM) + 0.5% glycerol v/v), conditions under which Tet repressor proteins are localized along the binding array. During these experiments, at time t = 9 s, the cell environmental conditions in the SCM are switched to media containing 200 ng mL^{-1} anhydrotetracycline (aTc). The presence of aTc induces the unbinding of TetR from the tandem array, followed by intracellular diffusion of TetR-Venus proteins (see Movie S5†). Using the SCM, we are able to observe the rapid release and subsequent intracellular diffusion of the Tet repressor within Gram-negative bacteria (Fig. 5), with a clear definition of the time at which the change in the surrounding medium occurs. Intracellular diffusion events were observed by incorporating a Dual View imaging system (Photometrics DV2) to simultaneously overlay phase-contrast and fluorescence images during data acquisition (see ESI†).

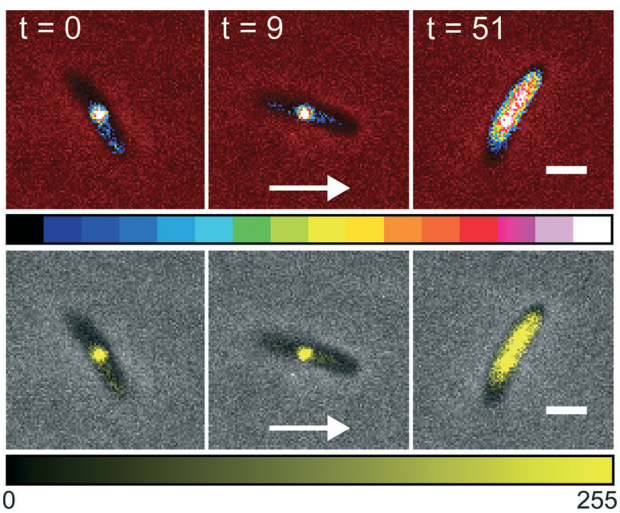

Fig. 5 Direct observation of intracellular diffusion of the Tet repressor after a single cell is rapidly transitioned to media containing 200 ng mL^{-1} aTc, which induces unbinding of TetR from a chromosomal binding array (see Movie S5†). Fluorescence images are shown in the top panel, with fluorescence intensity represented by a color scale (time t given in seconds). Phase-contrast images superimposed with fluorescence intensity are shown in the bottom panel. Scale bar: 2 μm.

It is important to note that the SCM allows for a precise and accurate definition of the time point of release and motion of intracellular repressor proteins, which facilitates analysis of the diffusion process. Our platform enables the rapid exchange of cell environmental conditions while maintaining single cells in free solution, whereas alternative methods of observing these diffusion events mainly rely on surface-immobilized bacteria and exchanging the surrounding medium by rinsing flow-through channels.[10,16,54] Generally speaking, surface-immobilization techniques are contact based methods that rely on convection or diffusion for media exchange. The SCM allows for rapid exchange of media and fluid streams in free solution, which is a key advantage for single cell experiments.

Conclusions

The SCM allows for direct observation of the intracellular dynamics during rapid media exchange for single cells in free solution. This technique provides a new method for observing single cell growth in an on-chip fashion. In this way, the SCM truly enables a chemostatic environment for observing the growth of single cells, allowing for continuous delivery of fresh nutrients with continuous removal of metabolic waste. In addition, the SCM can be modified to incorporate a bypass channel along one of the outlet flow channels for subsequent cell sorting of target cells. In prior work, we demonstrated the cell sorting capabilities of the SCM by targeting and separating morphologically distinct cells from heterogeneous ecological cell samples. In brief, a second set of on-chip pneumatic valves can be actuated to direct a trapped cell into the bypass sorting chamber for post-analysis or off-chip collection and processing.

In this work, we used the SCM to observe cell growth for long time scales (~5 cell divisions) and across several generations of daughter cells. In this way, the SCM allows for cell growth dynamics to be characterized for the full lineage of a single cell, with measurements of growth over successive generations for cells grown in free solution. Interestingly, our results suggest that as cells adapt to the chemostatic growth environment in the SCM, the average growth rates increase with subsequent generations. Moreover, the SCM facilitates stable confinement of motile bacteria, which attempt to actively swim away from the trap center during cell growth and confinement experiments. We have readily observed heightened levels of motility for cells cultured in minimal media (M9) compared to cells cultured in rich media (RDM).

Nevertheless, the SCM successfully confines motile cells upon tuning the controller gain constant to counteract enhanced cell motility.

In addition to cell growth measurements, the SCM allows for direct characterization of intracellular fluorescence levels and gene expression as a function of the dynamic cell growth environment. Here, we incorporate phase-contrast imaging and TLFM to simultaneously observe cell phenotype and intracellular fluorescence levels over time. In this work, we use the SCM to induce single step changes and time-dependent, periodic step changes in the cell growth medium while confining and observing a single cell in free solution and maintaining a constant total volumetric flow rate. During these experiments, cell division events are clearly observed within dynamic trajectories. These experiments serve as proof-of-principle validation of the SCM for characterizing gene expression and cell growth.

Finally, we used the SCM to directly observe intracellular diffusion of transcription factor proteins following a rapid change in the cell growth environment. In this way, the SCM effectively provides a new method for rapid on-demand nutrient switching while enabling observation of a 'target' cell in free solution. Importantly, the SCM allows for precise knowledge of 'time zero', or the time at which a cell is transitioned from one medium to a different medium. In our experiments, we used aTc as the stimulus to release Tet repressor proteins bound to a chromosomal binding array. Using this approach, we are able to control and subsequently observe the intracellular diffusive dynamics of the Tet repressor, thereby allowing for characterization of the spatial distribution of transcription factors in a target cell.

In comparison to alternative techniques, the SCM provides a fairly straightforward method for single cell analysis. Most labs conducting single cell research already incorporate fluorescence microscopy, and facilities for microfluidic fabrication are readily available. The main additional components required for the SCM are pressure regulators (Proportion Air) and LabVIEW software/hardware. These components can be obtained for a modest cost compared to other techniques that incorporate elaborate microfluidic networks or optical components.[43] In addition, trapping performance compares favorably with other techniques for single cell confinement because the hydrodynamic trapping force scales linearly with the particle radius (not volume), which enables facile confinement of small target particles, as discussed in prior work.[42]

In this work, we present an integrated two-layer microfluidic device capable of confining single cells for long time scales in free solution. The SCM is able to sustain constant nutrient conditions or periodic 'forcing' of well-defined growth media while allowing for direct analysis. Our technique allows for direct analysis of single cells confined in free solution, albeit at a relatively low throughput (one cell at a time). Clearly, it would be advantageous to develop a multiplexed bioreactor for high-throughput analysis of multiple cells. Future generations of the microfluidic trap can be built to facilitate the confinement of multiple cells (or arbitrary particles), though this technology will require a fairly substantial redesign of the microfluidic platform to accommodate multiple inlet and outlet channels and a more sophisticated feedback controller. Alternatively, trapping multiple cells (or particles) for shorter durations could be achieved by alternating the polarity of the compressional and extensional flow axes, analogous to implementing a Paul trap in aqueous solution.[55] In addition, trapping techniques with higher temporal resolution may require decoupling image acquisition with centroid detection by implementing hardware trapping for improved feedback latency as reported in methods such as optical[27] and electrophoretic techniques.[38]

Overall, the microfluidic bioreactor presented in this work provides a new method for sustaining or dynamically controlling environmental conditions, measuring growth rates, detecting gene expression, and observing intracellular dynamics in single cells suspended in free solution. In this way, the SCM is a valuable tool for the study and analysis of single cell dynamics.

Acknowledgements

We thank Prof. Paul J. A. Kenis and his group for providing access to cleanroom facilities for microdevice fabrication. We thank Arnab Mukherjee for help in cloning bacterial strains, Chris Brockman for help in implementing LabVIEW - EMCCD acquisition, and Folarin Latinwo for shear stress calculations and useful discussions. This work was funded by an NIH Pathway to Independence Award (4R00HG004183-03) and a Packard Fellowship for CMS, a National Science Foundation Graduate Research Fellowship Program for EMJC, and the National Science Foundation funded Center for the Physics of Living Cells (0822613) for TEK.

References

1 N. J. Guido, X. Wang, D. Adalsteinsson, D. McMillen, J. Hasty, C. R. Cantor, T. C. Elston and J. J. Collins, *Nature*, 2006, **439**, 856–860.
2 L. Cai, N. Friedman and X. S. Xie, *Nature*, 2006, **440**, 358–362.
3 M. L. Kovarik and N. L. Allbritton, *Trends Biotechnol.*, 2011, **29**, 222–230.
4 M. L. Kovarik, P. K. Shah, P. M. Armistead and N. L. Allbritton, *Anal. Chem.*, 2013, **85**, 4991–4997.
5 S. K. Sia and G. M. Whitesides, *Electrophoresis*, 2003, **24**, 3563–3576.
6 H. Andersson and A. van den Berg, *Sens. Actuators, B*, 2003, **92**, 315–325.
7 T. Vilkner, D. Janasek and A. Manz, *Anal. Chem.*, 2004, **76**, 3373–3385.
8 C. J. Ingham and J. E. T. van Hylckama Vlieg, *Lab Chip*, 2008, **8**, 1604–1616.
9 M. R. Bennett and J. Hasty, *Nat. Rev. Genet.*, 2009, **10**, 628–638.

10 A. Groisman, C. Lobo, H. Cho, J. K. Campbell, Y. S. Dufour, A. M. Stevens and A. Levchenko, *Nat. Methods*, 2005, **2**, 685–689.
11 M. A. Unger, H. P. Chou, T. Thorsen, A. Scherer and S. R. Quake, *Science*, 2000, **288**, 113–116.
12 M. Tanyeri, M. Ranka, N. Sittipolkul and C. M. Schroeder, *Lab Chip*, 2011, **11**, 4181–4186.
13 B. Meier, A. Zielinski, C. Weber, D. Arcizet, S. Youssef, T. Franosch, J. O. Rädler and D. Heinrich, *Proc. Natl. Acad. Sci. U. S. A.*, 2011, **108**, 11417–11422.
14 M. Hosokawa, T. Hayashi, T. Mori, T. Yoshino, S. Nakasono and T. Matsunaga, *Anal. Chem.*, 2011, **83**, 3648–3654.
15 Y. Wang, P. Shah, C. Phillips, C. E. Sims and N. L. Allbritton, *Anal. Bioanal. Chem.*, 2012, **402**, 1065–1072.
16 Z. Long, E. Nugent, A. Javer, P. Cicuta, B. Sclavi, M. Cosentino Lagomarsino and K. D. Dorfman, *Lab Chip*, 2013, **13**, 947–954.
17 E. Roberts, A. Magis, J. O. Ortiz, W. Baumeister and Z. Luthey-Schulten, *PLoS Comput. Biol.*, 2011, **7**, e1002010.
18 M. Assaf, E. Roberts and Z. Luthey-Schulten, *Phys. Rev. Lett.*, 2011, **106**, 4.
19 B. W. Andrews, T.-M. Yi and P. A. Iglesias, *PLoS Comput. Biol.*, 2006, **2**, e154.
20 D. Di Carlo, L. Y. Wu and L. P. Lee, *Lab Chip*, 2006, **6**, 1445–1449.
21 D. Di Carlo and L. P. Lee, *Anal. Chem.*, 2006, **78**, 7918–7925.
22 J. R. Rettig and A. Folch, *Anal. Chem.*, 2005, **77**, 5628–5634.
23 R. M. Johann, *Anal. Bioanal. Chem.*, 2006, **385**, 408–412.
24 B. R. Lutz, J. Chen and D. T. Schwartz, *Anal. Chem.*, 2006, **78**, 5429–5435.
25 K. C. Neuman and S. M. Block, *Rev. Sci. Instrum.*, 2004, **75**, 2787–2809.
26 A. Ashkin, J. M. Dziedzic, J. E. Bjorkholm and S. Chu, *Opt. Lett.*, 1986, **11**, 288–290.
27 T. L. Min, P. J. Mears, L. M. Chubiz, C. V. Rao, I. Golding and Y. R. Chemla, *Nat. Methods*, 2009, **6**, 831–835.
28 T. L. Min, P. J. Mears, I. Golding and Y. R. Chemla, *Proc. Natl. Acad. Sci. U. S. A.*, 2012, **109**, 9869–9874.
29 K. C. Neuman, E. H. Chadd, G. F. Liou, K. Bergman and S. M. Block, *Biophys. J.*, 1999, **77**, 2856–2863.
30 M. P. Landry, P. M. McCall, Z. Qi and Y. R. Chemla, *Biophys. J.*, 2009, **97**, 2128–2136.
31 S. Ayano, Y. Wakamoto, S. Yamashita and K. Yasuda, *Biochem. Biophys. Res. Commun.*, 2006, **350**, 678–684.
32 S. Umehara, I. Inoue, Y. Wakamoto and K. Yasuda, *Biophys. J.*, 2007, **93**, 1061–1067.
33 M.-C. Kim, Z. Wang, R. H. W. Lam and T. Thorsen, *J. Appl. Phys.*, 2008, **103**, 044701.
34 A. Chandrasekaran and M. Packirisamy, *IET Nanobiotechnol.*, 2008, **2**, 39–46.
35 C. M. Lin, Y. S. Lai, H. P. Liu, C. Y. Chen and A. M. Wo, *Anal. Chem.*, 2008, **80**, 8937–8945.
36 B. G. Hosu, K. Jakab, P. Banki, F. I. Toth and G. Forgacs, *Rev. Sci. Instrum.*, 2003, **74**, 4158–4163.
37 H. M. Hertz, *J. Appl. Phys.*, 1995, **78**, 4845.
38 A. E. Cohen and W. E. Moerner, *Appl. Phys. Lett.*, 2005, **86**, 93109.
39 A. Cohen, *Phys. Rev. Lett.*, 2005, **94**, 118102.
40 J. C. McDonald and G. M. Whitesides, *Acc. Chem. Res.*, 2002, **35**, 491–499.
41 M. Tanyeri, M. Ranka, N. Sittipolkul and C. M. Schroeder, *Lab Chip*, 2011, **11**, 1786–1794.
42 M. Tanyeri, E. M. Johnson-Chavarria and C. M. Schroeder, *Appl. Phys. Lett.*, 2010, **96**, 224101.
43 E. M. Johnson-Chavarria, M. Tanyeri and C. M. Schroeder, *J. Visualized Exp.*, 2011, 1–5.
44 G. K. Batchelor, *An Introduction to Fluid Dynamics (Cambridge Mathematical Library)*, Cambridge University Press, 2000.
45 D. E. Seborg, T. F. Edgar and D. A. Mellichamp, *Process Dynamics and Control*, Wiley, 2003.
46 C. Brockman, S. J. Kim and C. M. Schroeder, *Soft Matter*, 2011, **7**, 8005.
47 M. Tanyeri and C. M. Schroeder, *Nano Lett.*, 2013, **13**, 2357–2364.
48 K. M. Fridley, M. A. Kinney and T. C. McDevitt, *Stem Cell Res. Ther.*, 2012, **3**, 45.
49 F. K. Balagaddé, L. You, C. L. Hansen, F. H. Arnold and S. R. Quake, *Science*, 2005, **309**, 137–140.
50 M. B. Miller and B. L. Bassler, *Annu. Rev. Microbiol.*, 2001, **55**, 165–199.
51 A. R. Abate, D. Lee, T. Do, C. Holtze and D. A. Weitz, *Lab Chip*, 2008, **8**, 516–518.
52 T. E. Kuhlman and E. C. Cox, *Nucleic Acids Res.*, 2010, **38**, e92.
53 T. E. Kuhlman and E. C. Cox, *Bioeng. Bugs*, 2010, **1**, 296–299.
54 M. R. Bennett, W. L. Pang, N. A. Ostroff, B. L. Baumgartner, S. Nayak, L. S. Tsimring and J. Hasty, *Nature*, 2008, **454**, 1119–1122.
55 W. Guan, S. Joseph, J. H. Park, P. S. Krstic and M. A. Reed, *Proc. Natl. Acad. Sci. U. S. A.*, 2011, **108**, 9326–9330.

